Anisotropic geophysical vortices

James C. McWilliams
Geophysical Turbulence Program, NCAR, Boulder, Colorado 80307

Jeffrey B. Weiss
Program in Atmospheric and Oceanic Sciences, Astrophysical, Planetary, and Atmospheric Sciences, University of Colorado, Boulder, Colorado 80309

(Received 4 February 1994; accepted for publication 8 April 1994)

A survey is made of many types of coherent vortices in the Earth's ocean and atmosphere. These vortices often occur with strong, environmentally induced anisotropy in their velocity and vorticity fields. We propose a definition of the essential characteristics of coherent vortices and formulate hypotheses concerning their dynamical role in complex, anisotropic fluid motions. Finally, we analyze numerical solutions both for uniformly rotating, stably stratified three-dimensional flow and for two-dimensional flow for the phenomena of enstrophy cascade and dissipation, intermittency, isotropy in the appropriate coordinate frame, coherent vortex emergence, vortex population dynamics, and approach to a nonturbulent end state.

I. INTRODUCTION

From the contents of this journal issue, it is evident that highly organized vortex motions occur frequently in nature. Indeed, this topic comprises a vast scientific literature. In this essay we focus on the vortices of the Earth's ocean and atmosphere which are influenced by anisotropy in their large-scale environment. Among the most important environmental influences are rotation, stable stratification, and mean velocity shear. A manifestation of these influences is that the velocity vector field itself becomes anisotropic, such that one component is appreciably weaker than the other two. Under these conditions, the degree of vortex coherence is particularly strong, even in the turbulent flow fields of nature.

We illustrate the phenomenon by surveying a variety of coherent vortex motions in the Earth's atmosphere and ocean. Out of these examples we attempt to define the essential characteristics of vortex coherence, as well as a relevant measure of environmentally induced anisotropy. We then consider the particular idealized example of a statistically homogeneous, turbulent flow in a uniformly rotating and stably stratified environment. This situation presently provides perhaps the best combination of physical realism, theoretical understanding, and skillful numerical modeling for coherent vortices in turbulence. We also consider the analogy between this anisotropic 3-D flow and the less realistic but even simpler 2-D flow.

II. COHERENT VORTICES IN THE OCEAN AND ATMOSPHERE

Coherent vortices are common in nature, at both large and small scales. To illustrate this, we present several examples and briefly comment on their generation and behavior; however, no attempt is made to be comprehensive.

Velocity shear often is unstable, and the finite-amplitude outcome can be isolated vortices that are circularly symmetric about an axis perpendicular to both the mean velocity and its gradient. This is particularly clear when the shear occurs in a narrow layer. A well-known laboratory example is the Kármán vortex street for flow past an obstacle; its geophysical analogs are atmospheric flow past island orography, where vortices are evident in stratus cloud patterns, and oceanic flow past undersea topography, where vortices are evident in sea-surface surfactant patterns (Fig. 1). This vortex generation mechanism also occurs in unstable free-shear layers, both in the laboratory (Brown and Roshko, 1974) and in geophysical frontal flows; an example of the latter is seen in sea-surface temperature patterns (Flamant and Armi, 1985; Washburn and Armi, 1988). When the velocity shear occurs in a relatively broad layer, the vortices that arise do not have such a rigid axis of symmetry. Consequently they are often referred to as hairpin or horseshoe vortices, indicative of deformations of the axis of recirculation away from its ambient direction. Hairpin vortices occur frequently in stress-driven planetary boundary layers in association with the "sweeps and bursts" of flow, towards and away from the boundary, that effect the requisite momentum flux (e.g., Mahrt, 1991; Mahrt and Gibson, 1992).

In buoyancy-driven planetary boundary layers, the dominant coherent structures are buoyant plumes, which are seen as cumulus clouds in the atmosphere and, more indirectly, as convection remnants, called chimneys, in the ocean (Killworth, 1983). Chimneys are appreciably influenced by the Earth's rotation, so they end up, through a process called adjustment, with a geostrophically balanced, horizontally circulating flow. In this configuration they can persist for periods of months or even years. This process of vortex generation through adjustment towards a so-called balanced state is quite general: a local anomaly in the density or momentum field causes a vortical circulation to spin up yielding Coriolis or centrifugal forces to balance the implied pressure gradient forces. Adjustment following localized mixing events produces many types of anticyclonic, submesoscale coherent vortices in the ocean interior (McWilliams, 1985). These vortices are often detected through their locally anomalous chemical concentrations. The anomalies arise as the vortices travel large distances to regions with average concentrations different than those at their creation sites, while the fluid trapped in their interiors largely retains the original concentrations. Another example of vortices generated through ad-

 1054-1500/94/4(2)/305/7/$6.00

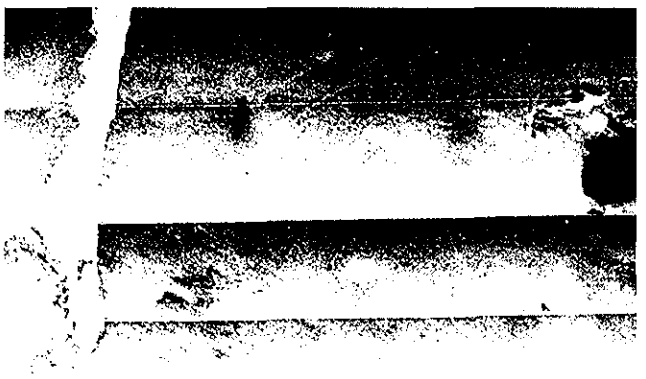

FIG. 1. Synthetic aperture radar images of island-shed vortices near the Bahamas (courtesy of B. Holt, JPL).

justment is low-density, river-outflow water that ends up in circular, convex-lens configurations trapped against the sea surface with anticyclonic vortical flow (Nof, 1981). Dipole pairs can arise out of adjustment of local, unidirectional momentum impulses; these are frequently seen in sea surface temperature and color images and are called mushroom vortices because of the pattern they create in passive tracer fields (Fedorov and Ginsberg, 1986; Mied *et al.*, 1991).

When vertical shear of horizontal velocity occurs in a stably stratified fluid on scales large enough to be influenced by planetary rotation, it can be baroclinically unstable. Vortical products of this instability include the familiar synoptic-scale cyclones of the extra-tropical atmosphere and oceanic vortices seen in the marginal ice zones (Fig. 2). The meandering jet instability of the Gulf Stream, yielding long-lived Rings, is also at least partly of this type (horizontal shear also contributes to the instability).

Another potent means of producing coherent vortices is by the intensification of the ambient vorticity by suction-induced inflow. This is the cause of the intense winds that develop in hurricanes and tropical cyclones, as well as in tornados on a somewhat smaller scale, and in dust devils and water spouts on even smaller scales. Also, photographs of sun-glint patterns from space show many spiral eddy patterns on the ocean surface (personal communication from Scully-Powers, NASA), which are probably the result of surfactants organized by boundary-layer inflow in small cyclonic vortices.

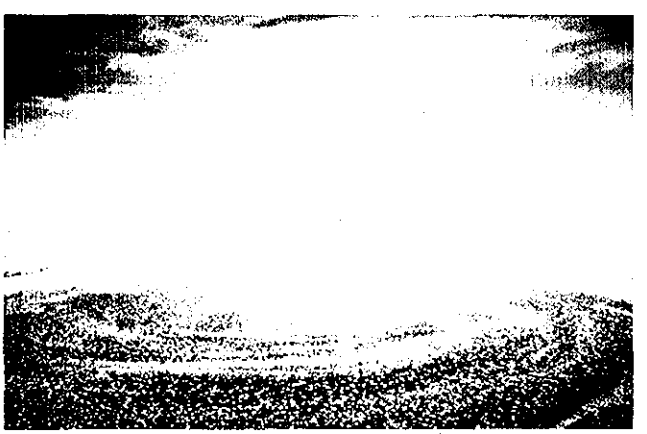

FIG. 2. Photograph of vortices in the marginal ice zone near Greenland (from Johannessen *et al.*, 1992).

Whatever their generation process, an important property of coherent vortices is their persistence as quasistationary flow configurations, with neither strong forcing nor dissipation required to maintain them. Well known examples of this are the following: long-lived vortices in the planetary-scale shear flows on the Gas Giant planets; dipolar or omega blocking patterns in the Earth's atmospheric westerly winds; cutoff, occluded low-pressure patterns found on the tropical side of the jet stream; and the stratospheric polar night vortices which act as hermetic incubators for the clouds and chemical reactions that create the seasonal ozone holes.

This survey indicates the abundance of coherent vortices in nature. Yet these examples are just the vortices that are either big or strong enough not to be overlooked, or else discernible by chance (usually through some material tracer), and so they have been given names. Undoubtedly, there are many more types yet to be found and named.

III. ATTRIBUTES OF COHERENT STRUCTURES

Humans have an innate proficiency in pattern recognition, which is the original basis for identification of coherent structures. Mathematization of this skill, however, is a more difficult cognitive task. This requires a definition of a coherent structure; here we propose several elements that we believe should be included.

The term was first used by Brown and Roshko (1974) to describe large, quasi-2-D vortices they saw by flow visualization of a free-shear layer. The word structure suggests something which is a single recognizable entity, while the adjective coherent adds the idea of a logical ordering of the component parts. The presence of coherent structures is in marked contrast to the concept of turbulence as random, formless flow. Brown and Roshko rightly suspected that these vortices are particularly important in the dynamics of this regime of turbulence.

In the intervening 20 years, many other examples of coherent structures have been presented (e.g., Métais and Lesieur, 1989), and we have given some geophysical examples above. From this collection, we can identify several attributes of coherent structures. These attributes are meant to be both descriptive and definitional. They comprise at most a working definition, based upon substantial experience but subject to modification as we learn more about coherent structures.

A. A recurrent, spatially localized pattern in the field variables

The spatial locality of a coherent structure implies global correlations in the spectrum, contradicting the traditional picture of turbulence as a local cascade in wave-number space. The orderliness of the pattern is often most apparent in the vorticity (or potential vorticity) field, which supports "coherent vortex" as a frequent synonym.

B. A preferred state with respect to the nonlinear dynamics

Coherent structures are flow configurations close to stationary or self-similarly evolving states of the conservative, nonlinear fluid dynamical equations. Furthermore, these states are stable with respect to small perturbations in these dynamics. Coherent structures are dynamically self-organizing, attracting patterns, which develop through advection (dissipative, nonlinear turbulent cascade) and/or adjustment (conservative wave emission).

C. Long-lived in a Lagrangian reference frame

The longevity is in comparison to a typical Eulerian time scale, such as an Eulerian autocorrelation time or an eddy recirculation time. A coherent structure is thus at most weakly dissipative over most of its lifetime. Its long lifetime enables it to move significant distances before surrendering its contents, making it capable of "anomalous transport" of material properties; this is in contrast to dispersion by random walks with mixing-length step sizes.

D. Spatially isolated from other coherent structures during most of its lifetime

Because of their typically large spatial separation, coherent vortices are only weakly disturbed by each other. However, close encounters do occur, albeit rarely. This can result in transformation and even destruction of the structures themselves, often accompanied by significant bursts of dissipation. These rare events are a likely source of the statistical intermittency that has long been recognized as a fundamental property of turbulent flows, a property which is typically difficult to explain from the classical views of universal cascade, statistical equilibrium, or stochastic closure theories.

A reason for being tentative about constructing a rigorous definition of coherent structures is that distinguishing them from other flow configurations can sometimes be subtle. How, for example, does one identify the boundary of a coherent structure in a complex flow field, or distinguish between a weak, short-lived, or deformed coherent structure and a strong, random fluctuation? Another reason is that information about coherent structures can often be hard to come by: they are sparse patterns in the field variables, thus requiring multidimensional and perhaps multivariate data of long duration; they are best seen in vorticity or potential vorticity, which is not an easily measured quantity in nature or the laboratory; and they are creatures of high Re, thus requiring large laboratory or computational devices to be realized outside of nature. Because of these difficulties in their detection, almost certainly the abundance and variety of coherent structures in the ocean and atmosphere is much greater than can now be demonstrated.

IV. ANISOTROPY AND COHERENCE

In all of the geophysical examples in Sec. II, the velocity field is at least locally anisotropic; furthermore, in all but the small-scale convective plumes and broad-shear-layer hairpin vortices, the anisotropy has a global Cartesian coordinate orientation, such that

$$w \ll u, v, \tag{1}$$

where z, w are the "vertical" coordinate and velocity component and (x,y), (u,v) are their "horizontal" counterparts. A consequence of (1) is that the 3-D incompressibility condition becomes approximately a horizontal, 2-D one with an associated streamfunction, ψ:

$$u_x + v_y \approx 0 \Rightarrow u \approx -\psi_y, \quad v \approx \psi_x. \tag{2}$$

Another consequence is that the dominant vorticity component is the vertical one, ζ, where

$$\zeta = v_x - u_y = \psi_{xx} + \psi_{yy}. \tag{3}$$

When is this type of velocity anisotropy likely to occur? It occurs when the characteristic velocity V and length scale L of the flow combine to make a frequency which is smaller than that characterizing the anisotropic environment, ω; i.e.,

$$\epsilon \equiv \frac{V}{\omega L} \ll 1. \tag{4}$$

Among the most important environmental influences are rotation, stable stratification, and velocity shear. In the case of rotation, $\omega \equiv f = 2\boldsymbol{\Omega}\cdot\hat{\mathbf{z}}$, where f is the Coriolis frequency and $\boldsymbol{\Omega}$ is the rotation vector of the local environment, which is often the Earth itself; here ϵ is called the Rossby number, Ro. For stratification, $\omega \equiv N^2 = \mathbf{g}\cdot\nabla \ln\bar{\rho}$, where N is the Brunt–Väisälä frequency, $\mathbf{g}$ is the gravitational acceleration vector, $\bar{\rho}$ is the mean density profile; here ϵ is called the Froude number, Fr. For the case of shear, $\omega = |\nabla \times \bar{\mathbf{u}}|$, where $\bar{\mathbf{u}}$ is the mean velocity profile.

For rotation and stratification, neither of which can be a source for generating turbulence, ϵ can be arbitrarily small, and the degree of velocity anisotropy can be arbitrarily large. In contrast, velocity shear is usually unstable at large Reynolds number, Re, and thus is a source of turbulence. In equilibrium, therefore, V is proportional to ωL, and ϵ is not an externally controllable parameter, although it typically is less than one. For shear in narrow layers or shear in combination with rotation or stratification, velocity anisotropy occurs to a substantial degree; this is the situation for most of the geophysical examples above. For broad shear alone, where hairpin vortices are the coherent structures, the situation is more ambiguous: $\epsilon \approx 0.4$, ζ is the dominant component of vorticity (but only barely), and the velocity component ordering is more nearly $u \gg v, w$, where u is the component in the direction of the mean flow (Champagne *et al.*, 1970; Rogers and Moin, 1987). In a completely isotropic environment, the coherent structures are elongated tubes of concentrated vorticity with quite narrow diameters that arise through the process of vortex stretching (She *et al.*, 1990; Vincent and Meneguzzi, 1993). Of course, in this case the turbulent flow must be globally isotropic, and only in local neighborhoods can (1)–(3) be satisfied, with $\hat{\mathbf{z}}$ parallel to the local tube axis.

We propose two hypotheses with regard to the nature of coherent structures in complex flow environments. The first concerns their occurrence and dynamical importance:

* Turbulent fluid motions at large Re develop coherent structures whose dynamics govern the aggregate properties of the flow such as transport and dissipation.

The second concerns the role of velocity anisotropy:

* For more anisotropic velocity fields, the coherent structures have weaker vortex stretching, occur on larger spatial scales, contain a greater fraction of the enstrophy, and thus exercise a greater degree of dynamical control over the system evolution.

As we have seen above, there are many regimes of geophysical turbulence, and in each of them the degree of validity of these hypotheses will have to be examined before we can accept them. Although much effort has been directed to these examinations in recent years, the inquiry is far from complete.

V. ANISOTROPIC TURBULENCE

We now examine the hypotheses of the preceding section for two canonical examples of anisotropic turbulence: the geophysically relevant situation of 3-D, rotating, stably stratified flow and the most extreme form of the velocity anisotropy condition (1), viz., 2-D flow. In both these cases homogeneous, isotropic, random initial conditions develop into coherent vortices which subsequently dominate the flow evolution. For simplicity we pose these examples with the greatest possible symmetries.

Rotating, stratified flow has an asymptotic dynamics as Ro,Fr$\to$0 called quasigeostrophy (QG) (Pedlosky, 1987). This is an anisotropic geophysical flow regime, both because (1) is true and because QG typically applies to horizontal scales larger than the fluid depths of the Earth's ocean and atmosphere. If we assume that f and N are spatially uniform, then both frequencies can be removed from the QG equations by a coordinate transformation $Nz/f\to z$:

$$q_t+J(\psi,q)=-\nu\nabla^4 q, \quad q=\nabla^2\psi, \tag{5}$$

where q is the potential vorticity, ∇ is the 3-D gradient operator, J is the horizontal Jacobian operator $[J(A,B) = A_xB_y-A_yB_x]$ representing horizontal advection, and ν is a hyperviscosity. For $\nu=0$, QG has two quadratic integral invariants, energy and enstrophy:

$$E=\frac{1}{2\mathcal{V}}\int d\mathbf{x}|\nabla\psi|^2, \quad V=\frac{1}{\mathcal{V}}\int d\mathbf{x}\, q^2, \tag{6}$$

where $\mathcal{V}$ is the volume of the domain.

Except for the advection operator, the transformed QG equations (5) and their invariants (6) are spatially isotropic. This isotropy is only possible because the anisotropies in velocity and geometric aspect ratio have already been accounted for in deriving (5). Charney (1971) proposed that the QG solutions therefore would also be isotropic, at least in a statistical average. In this case q and ψ would be isotropic functions of their coordinates in the stretched coordinate frame used in (5), while other quantities such as velocity are still anisotropic. We shall refer to this limited kind of isotropy as geostrophic isotropy. To investigate the self-consistency of geostrophic isotropy, we pose our examples with isotropic initial conditions and domain size.

Charney also made predictions for the evolutionary tendencies of QG flow, based upon its analogy with 2-D flow. The mathematical form of this analogy is that (5)–(6) also represent 2-D flow if ∇ and $(1/\nu)\int d\mathbf{x}$ are interpreted as 2-D operators. (Note that $q=\zeta$ in 2-D.) To investigate this analogy, we pose parallel problems for (5) in 3-D and 2-D and compare their solutions.

There is great qualitative similarity in the expected behaviors of QG and 2-D. The two quadratic invariants (6) imply that any evolutionary tendency to broaden the wavenumber spectrum—which some might consider an operational definition of turbulence—must be accompanied by $E(k)$ being transferred preferentially towards larger scales and $V(k)$ towards smaller ones. Under the isotropy hypothesis, it is these wave-number cascades which act to keep the spectrum isotropic (Batchelor, 1953; Charney, 1971). In the presence of viscous dissipation on very small scales, these transfer tendencies lead to vanishingly small energy dissipation as Re$\to\infty$ but finite enstrophy dissipation. The time scale for evolution of the spectrum is the nonlinear advection time, $t_a\sim Z^{-1/2}$, where Z is the variance of ζ. The time scale for significant enstrophy dissipation is $t_d\sim t_a$ log[Re] (Lesieur, 1990), which can be only a modest multiple of t_a even for large Re. In association with the occurrence of significant enstrophy dissipation, coherent vortices emerge from the random initial conditions, and thereafter the dissipation diminishes as the enstrophy contained within the vortices is protected from cascade to small scales (McWilliams, 1990a). The population of vortices evolves through nonconservative interactions, becoming progressively fewer, larger, more sparsely distributed, having less frequent close encounters, and exhibiting greater intermittency (McWilliams, 1984, 1989, 1990b, 1990c; McWilliams *et al.*, 1994). This continues until an approximate end-state configuration is achieved that has no further dissipative nonlinear evolution (Matthaeus *et al.*, 1991; Carnevale *et al.*, 1992; McWilliams *et al.*, 1994). Given these qualitative similarities in behavior, we now consider how quantitatively close the 2-D and QG evolutions are for the parallel problems posed above.

The parallel problems are the evolution in (5) from homogeneous, isotropic, random-phase initial conditions. The domain extent is 2π, the boundary conditions are periodic, and the computational grid size is $N=256$ in each direction. The initial energy is $E=1$, and the spectrum shape is peaked at intermediate scales with a relatively narrow bandwidth: $E(k) \propto k^\alpha/(k^{2\alpha}+k_0^{2\alpha})$, where k is the wavenumber modulus, $\alpha=10$, and $k_0=17.5$. A common initial $E(k)$ implies that the enstrophy $V(k)=2k^2E(k)$ is also initially the same. To examine weak decay at large Re, we use a small hyperviscosity, $\nu=3\times10^{-8}$. The only nonparallel feature, for reasons of convenience, is that we use an implicit, finite-difference, multigrid solver in 3-D (Yavneh *et al.*, 1994) and an explicit pseudospectral solver in 2-D (Orszag, 1971); however, we believe that this difference is not important in the analyses below.

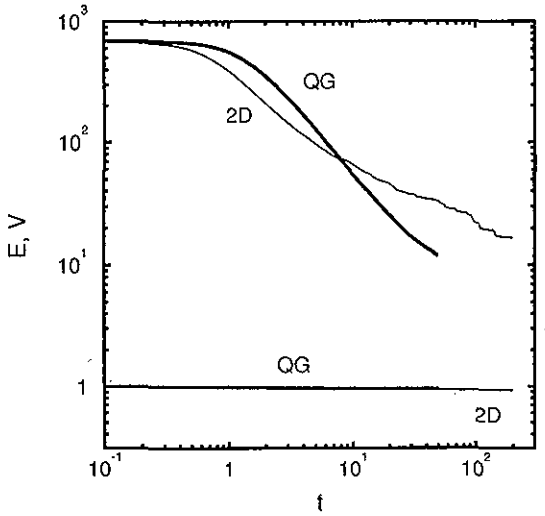

FIG. 3. Energy E (lower curves) and enstrophy V (upper curves) for 2-D (thin lines) and QG (thick lines).

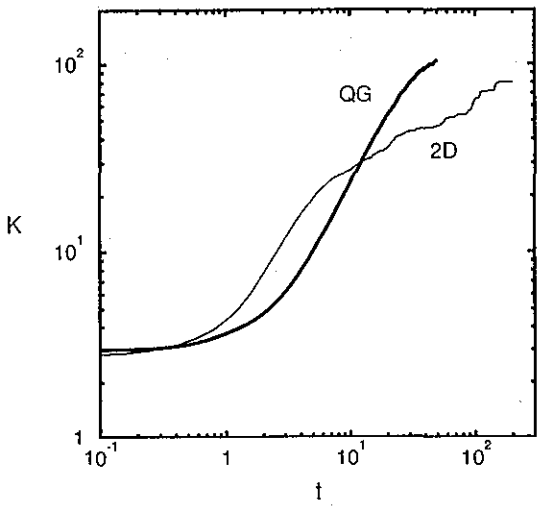

FIG. 5. Potential vorticity kurtosis K for 2-D (thin line) and QG (thick line).

A. Cascade and dissipation

In Fig. 3 are time series of the inviscid invariants, E and V. In 2-D the initial enstrophy gives an initial $Z^{-1/2}(0)=0.038$, while in QG $Z^{-1/2}(0)=0.052$ (for a 3-D, isotropic, narrow-band spectrum $Z=\frac{8}{15}V$). Energy is nearly conserved in both 2-D and QG, even over an interval of many hundreds of t_a, while enstrophy decays quite substantially over this interval. Figure 4 shows the enstrophy dissipation, $-dV/dt$. The dissipation begins earlier in 2-D than in QG, and it reaches a peak at $t\approx 0.6$ in 2-D, compared to $t\approx 1.1$ in QG. Thus, the above estimate of t_d is roughly confirmed, but its value for QG is even larger than can be explained by the differences in $Z(0)$. Isotropic wave-number spectra (i.e., shell integrals of the squared amplitude of the Fourier transform of q at constant wave-number modulus, $k=|\mathbf{k}|$) show that the 2-D spectrum broadens more rapidly than QG at early times, even after scaling by $Z^{-1/2}$, which leads to its earlier, stronger dissipation.

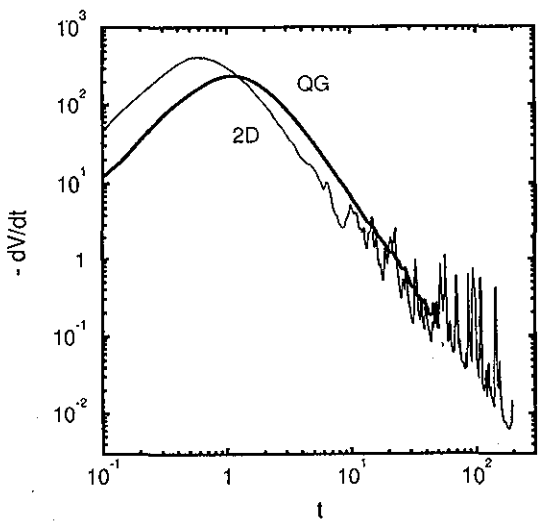

FIG. 4. Enstrophy dissipation, $-dV/dt$, for 2-D (thin line) and QG (thick line).

At later times after the peak of enstrophy dissipation, 2-D becomes less dissipative than QG (Fig. 4), enough so that V in QG eventually falls below its value in 2-D. Isotropic wave-number spectra at late times are much steeper at large k in 2-D, consistent with its smaller dissipation rate.

B. Intermittency

The temporal intermittency of the domain-integrated dissipation at late times is quite striking in 2-D, and it is much less so in QG (Fig. 4). We interpret this difference as primarily a dimensional difference: if temporal intermittency is associated with events on small scales, then there will be many fewer such events in a 2-D plane than in a 3-D volume in any given time period, so integral measures will be much more variable in 2-D. A direct measure of the spatial intermittency is the spatial kurtosis of q (Fig. 5),

$$K=\frac{1}{V^2\mathscr{V}}\int d\mathbf{x}\, q^4. \tag{7}$$

Its initial value is near the Gaussian value of 3, reflecting the random initial conditions. It starts to increase around the time of maximum enstrophy dissipation; thus, the increase begins earlier in 2-D. Thereafter, it steadily increases throughout the period of integration. At late times, QG shows even more spatial intermittency than 2-D, which also is partly a dimensional effect. Also, with kurtosis as with dissipation, we see greater temporal nonuniformity in the evolution of an integral measure in 2-D than in QG.

C. Tendency towards coordinate isotropy

Since the 2-D equations are formally symmetric with respect to an interchange of x,y, we have a firm expectation that its statistical dynamics will be fully isotropic. This expectation is confirmed by examination of its 2-D wave-

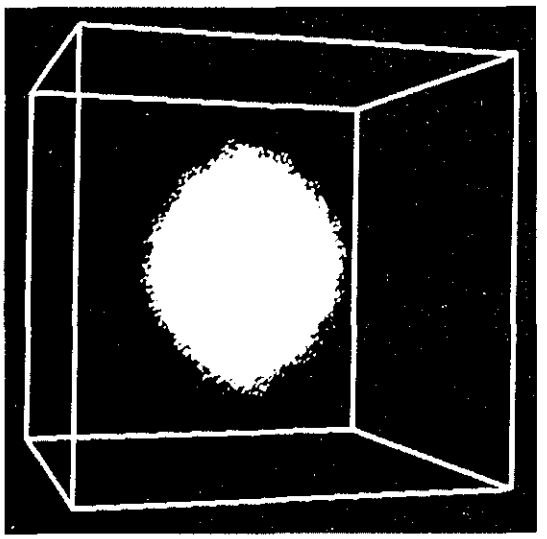

FIG. 6. A contour surface of the QG q spectrum in the wave-number range larger than the spectrum peak ($t=5.0$). The coordinate axes are $(k^{(x)},k^{(y)},k^{(z)})$, with $k^{(z)}$ up and $\mathbf{k}=0$ in the center of the box.

number spectra. In contrast, the Charney prediction of 3-D geostrophic isotropy has a much more heuristic basis, and, after the time of maximum dissipation, is quantitatively false: the 3-D spectrum shows $\mathcal{O}(1)$ departures from isotropy. Figure 6 shows a particular surface of constant spectrum amplitude; its elongation parallel to the vertical wavenumber axis indicates that typical flow structures on these scales have aspect ratios (height divided by breadth) less than one. An analysis in McWilliams *et al.* (1994) shows that this sense of spectrum anisotropy occurs throughout the wave-number range from the most energetic scales to the dissipation scales; at wave numbers smaller than the peak the spectrum is anisotropic in the opposite sense. Nevertheless, even though Charney's geostrophic isotropy prediction is not quantitatively accurate, it is qualitatively valid in that the 2-D horizontal advection in (5) does not cause gross discrepancies from 3-D coordinate isotropy in the coordinate frame $(x,y,Nz/f)$.

D. Vortex interactions and population evolution

In all of the preceding statistical measures, we see changes in the evolutionary behavior after the time of maximum dissipation: enstrophy dissipation diminishes (by definition), the spectrum steepens at large k, intermittency increases, and geostrophic anisotropy develops in QG. What is distinctive about this time is that it also is when coherent vortices become evident in the q fields; in particular, the dissipation of cascade-generated, filamentary structures in q leads to broad zones of weak q in between the emerging vortices. Thus, the statistical properties above are characteristic of the dynamical regime of vortex dominance of the flow evolution.

At the time of vortex emergence QG has more vortices than 2-D due to the three-dimensionality of the flow. The population evolution in QG is faster than 2-D, again due to dimensionality effects: there are more ways for vortices to approach closely in 3-D than in 2-D. In 2-D population evolution primarily results from the dissipative merger of two close same-sign vortices. In QG, this same phenomenon occurs when two vortices at roughly the same vertical level approach closely, but in addition, there is the phenomenon of alignment where vorticity at different levels lines up vertically, even within separate vortices (McWilliams, 1989; McWilliams *et al.*, 1994).

Figure 7 (Plate 6) shows the q field at time 20.4 both for 2-D and for QG in planer cross-sections and volume rendering (because of the opaque and hazy renderings in panels b and c, respectively). In a horizontal plane one sees fewer vortices and more vortex filaments in QG than in 2-D [Figs. 7(a) and 7(b), (Plate 6)], indicative of the faster vortex population evolution and greater dissipation (Fig. 4). However, there are more vortices overall in QG [Fig. 7(c) (Plate 6)], and their elemental shape is axisymmetric about $\hat{\mathbf{z}}$ and ellipsoidal with a preferred aspect ratio slightly less than one (cf. Sec. V C and Fig. 6). [This latter property is measured by the vortex census algorithm described in McWilliams, (1990c).] The vertical alignment of separate vortices can be seen in both the vertical cross-sections and the volume rendering.

In 2-D, the vortex population evolution can be understood in terms of scaling behaviors and punctuated Hamiltonian dynamics (Carnevale *et al.*, 1991; Benzi *et al.*, 1988, 1992; Weiss and McWilliams, 1993). Scaling behaviors are self-similar evolutions of the vortex population and integrated statistical measures (e.g., power-law regimes on Figs. 3–5), and punctuated Hamiltonian dynamics are simplified dynamical systems based upon the coherent vortices that combine intervals of conservative evolution with abrupt dissipative transformations. Although it is presently unknown whether QG can also be understood in these terms, we are optimistic. Qualitatively, the evolution of QG vortices is conservative motion interrupted by dissipative events. The difficulties lie in determining the correct singularization and transformation rules. While in 2-D only one dissipative interaction had to be included, merger of close, like-sign vortices, in QG one must account for both merger and alignment, at the least. The possibility of scaling behaviors for QG is still unsettled, but if it exists then the scaling exponents would be larger due to the faster population evolution seen in QG.

E. Vortex end states

The end-state of significantly dissipative nonlinear evolution occurs when all possible vortex amalgamations have taken place and the remaining vorticity configuration is close to an inviscid stationary state of the nonlinear dynamics. When the domain integrated vorticity is zero, as here, such states are dipolar configurations (sometimes called modons). Figure 8 (Plate 7) shows q approaching the end-states for both QG, at $t=50$, and 2-D, at $t=200$. The disparity in these times is again indicative of the faster vortex population evolution of QG compared to 2-D. As time progresses beyond these states the two columns in QG will sweep up the remaining isolated vortices into dipolar columns through both merger and alignment processes, while each pair of

same-sign vortices in 2-D will merge to form the final dipole. Note that in QG, the two columns have significant small scale structure resulting from the history of vertical alignment of individual vortices; the end-state is thus not fully barotropic although it does have a substantial depth-averaged component. Once the final dipole is reached, the remaining evolution is very slow diffusion to an ultimate state of rest.

VI. CONCLUSIONS

Because of the abundance and variety of coherent vortices in the ocean and atmosphere, it is an important challenge to develop better modeling skill and theoretical understanding of their dynamics and roles in the general circulation. In addressing this challenge, we believe it is fruitful both to focus on anisotropic flow regimes, where coherent behavior may be more pronounced, and to at least occasionally practice a comparative dynamics between distinct physical regimes. The comparison presented here between 3-D geostrophic and 2-D flows is an example of this. There are indeed very strong similarities in behavior, but there are also discernible differences in their rate-controlling processes that, at present, have only partly been explained.

ACKNOWLEDGMENTS

We appreciate the cooperation of our colleagues, Nancy Norton and Irad Yavneh. This work was supported by the National Science Foundation through the National Center for Atmospheric Research, the Pittsburgh Supercomputing Center, and HPCC-GCAG Grant No. ECS9217394.

Batchelor, G. (1953). *The Theory of Homogeneous Turbulence* (Cambridge University Press, Cambridge).

Benzi, R., Paternelo, S., and Santangelo, P. (1988). "Self-similar coherent structures in two-dimensional turbulence," J. Phys. A Gen. **21**, 1221–1237.

Benzi, R., Colella, M., Briscolini, M., and Santangelo, P. (1992). "A simple point-vortex model for decaying two-dimensional turbulence," Phys. Fluids A **4**, 1036–1039.

Brown, G. L., and Roshko, A. (1974). "On density effects and large structures in turbulent mixing layers," J. Fluid Mech. **64**, 775–816.

Carnevale, G. F., McWilliams, J. C., Pomeau, Y., Weiss, J. B., and Young, W. R. (1991). " Evolution of vortex statistics in two-dimensional turbulence," Phys. Rev. Lett. **66**, 2735–2737.

Carnevale, G. F., McWilliams, J. C., Pomeau, Y., Weiss, J. B., and Young, W. R. (1992). "Rates, pathways, and end-states of nonlinear evolution in decaying two-dimensional turbulence: Scaling theory vs. selective decay," Phys. Fluids A **4**, 1314–1316.

Champagne, F. H., Harris, V. G., and Corrsin, S. (1970). "Experiments on nearly homogeneous shear flow," J. Fluid Mech. **41**, 81–139.

Charney, J. G. (1971). "Geostrophic turbulence," J. Atmos. Sci. **28**, 1087–1095.

Fedorov, K.N., and Ginsberg, A. I. (1986), "Mushroom-like currents (vortex dipoles) in the ocean and in a laboratory tank," Ann. Geophys. B **4**, 507–516.

Flamant, P., and Armi, L. (1985). "A series of satellite images showing the development of shear instabilities," EOS **66** (27), cover photo and text.

Johannessen, O. M., Campbell, W. J., Shuchman, R., Sandven, S., Gloersen, P., Johannessen, J., Josberger, E. G., and Haugan, P. M. (1992). "Microwave study program of air-sea-ice ocean interactive processes in the seasonal ice zone of the Greenland and Barents Seas," in *Microwave Remote Sensing of Sea Ice*, edited by F. D. Carsey, American Geophysical Union Geophysical Monograph 68 (AGU, Washington, DC), pp. 261–289.

Killworth, P. D. (1983). "Deep convection in the world oceans," Rev. Geophys. **21**, 1–26.

Lesieur, M. (1990). *Turbulence in Fluids* (Kluwer Academic, Dordrecht), p. 281.

Mahrt, L. (1991). "Eddy asymmetry in the sheared heated boundary layer," J. Atmos. Sci. **48**, 472–492.

Mahrt, L., and Gibson, W. (1992). "Flux decomposition into coherent structures," Boundary-Layer Meteorol. **60**, 143–168.

Matthaeus, W. H., Stribling, W. T., Martinez, D., Oughton, S., and Montgomery, D. (1991). "Selective decay and coherent vortices in two-dimensional incompressible turbulence," Phys. Rev. Lett. **66**, 2731–2734.

McWilliams, J. C. (1984). "The emergence of isolated, coherent vortices in turbulent flow," J. Fluid Mech. **146**, 21–43.

McWilliams, J. C. (1985). "Submesoscale, coherent vortices in the ocean," Rev. Geophys. **23**, 165–182.

McWilliams, J. C. (1989). "Statistical properties of decaying geostrophic turbulence," J. Fluid Mech. **198**, 199–230.

McWilliams, J. C. (1990a). "A demonstration of the suppression of turbulent cascades by coherent vortices in two-dimensional turbulence," Phys. Fluids A **2**, 547–552.

McWilliams, J. C. (1990b). "The vortices of two-dimensional turbulence," J. Fluid Mech. **219**, 361–385.

McWilliams, J. C. (1990c), "The vortices of geostrophic turbulence," J. Fluid Mech. **219**, 387–404.

McWilliams, J. C., Weiss, J. B., and Yavneh, I. (1994). "Anisotropy and coherent structures in planetary turbulence," Science **264**, 410–413.

Métais, O., and Lesieur, M. (editors) (1989). *Turbulence and Coherent Structures* (Kluwer, Dordrecht).

Mied, R. P., McWilliams, J. C., and Lindemann, G. J. (1991). "The generation and evolution of mushroom-like vortices," J. Phys. Oceanogr. **21**, 489–510.

Nof, D. (1981). "On the dynamics of equatorial outflows with application to the Amazon's basin," J. Mar. Res. **39**, 1–29.

Orszag, S. (1971). "Numerical simulation of incompressible flow within simple boundaries. I. Galerkin (spectral) representation," Stud. Appl. Math. **50**, 293–328.

Pedlosky, J. (1987). *Geophysical Fluid Dynamics* (Springer, New York).

Rogers, M.M., and Moin, P. (1987). "The structure of the vorticity field in homogeneous turbulent flows," J. Fluid Mech. **176**, 33–66.

She, Z.-S., Jackson, E., and Orszag, S. (1990), "Intermittent vortex structures in homogeneous isotropic turbulence," Nature **344**, 226–228.

Vincent, A., and Meneguzzi, M. (1991). "The spatial structure and statistical properties of homogeneous turbulence," J. Fluid Mech. **225**, 1–20.

Washburn, L., and Armi, L. (1988). "Observations of frontal instabilities on an upwelling front," J. Phys. Oceangr. **18**, 1075–1092.

Weiss, J. B., and McWilliams, J. C. (1993). "Temporal scaling behavior of two-dimensional turbulence," Phys. Fluids A **5**, 608–621.

Yavneh, I., McWilliams, J. C., and Norton, N. J. (1994). "Multigrid solution to the quasigeostrophic equations" (in preparation).

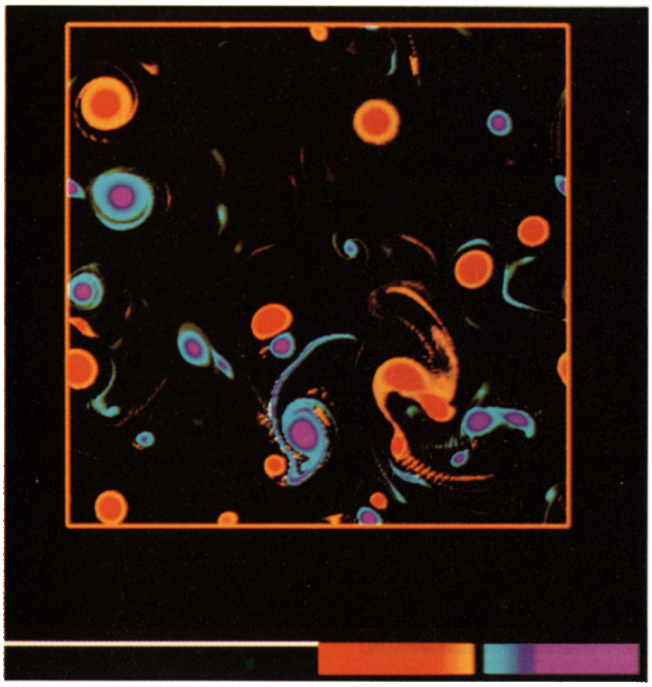

(a)

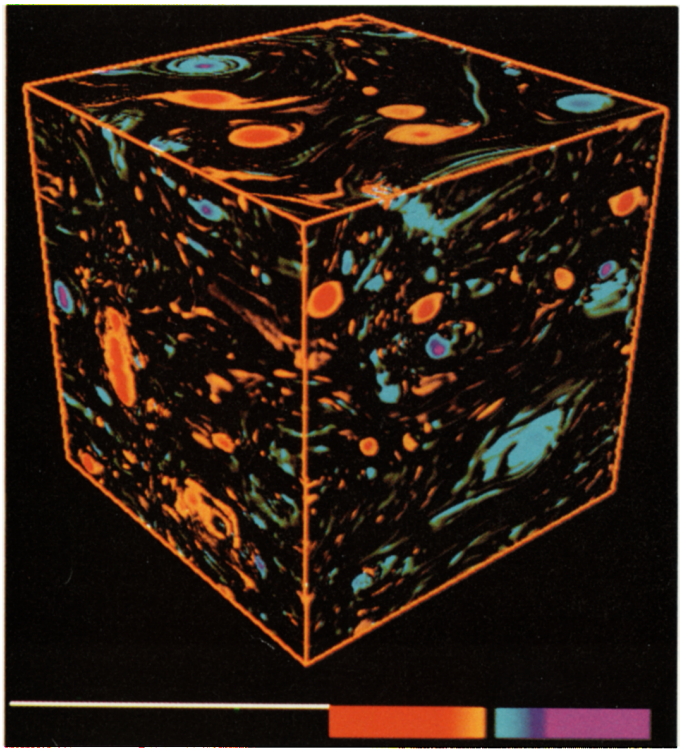

(b)

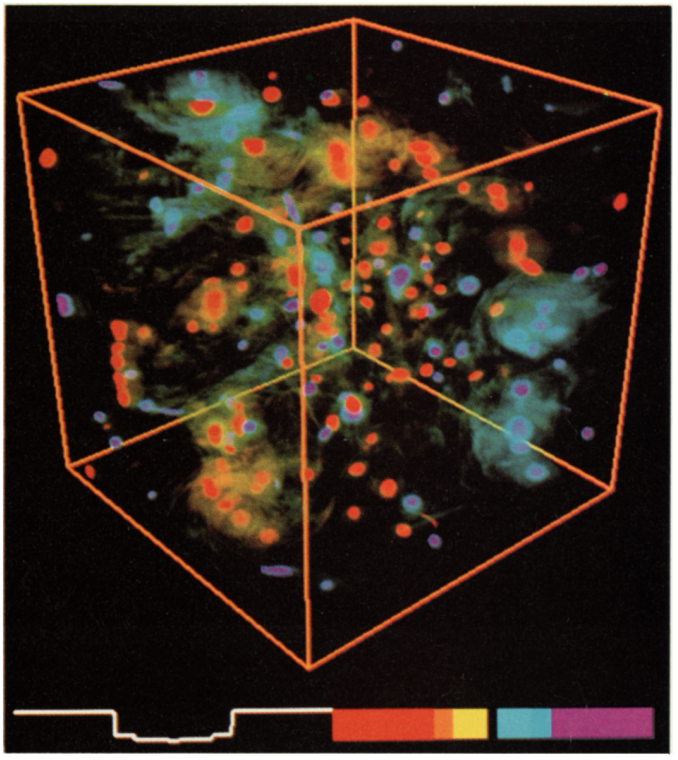

(c)

FIG. 7. q visualization at $t=20.4$: (a) 2-D in its plane with opaque rendering, (b) QG in its volume with opaque rendering, and (c) QG in its volume with hazy rendering. The curves beneath the images show the opacity (left; high values indicate opaqueness, low ones transparence) and hue (right) as a function of q, centered about $q=0$.

J. C. McWilliams and J. B. Weiss (see page 310)

PLATE 7

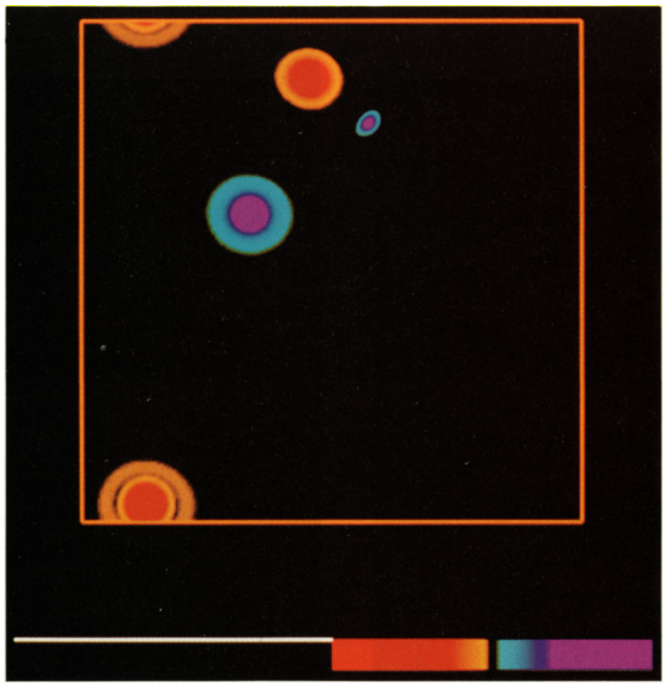

(a)

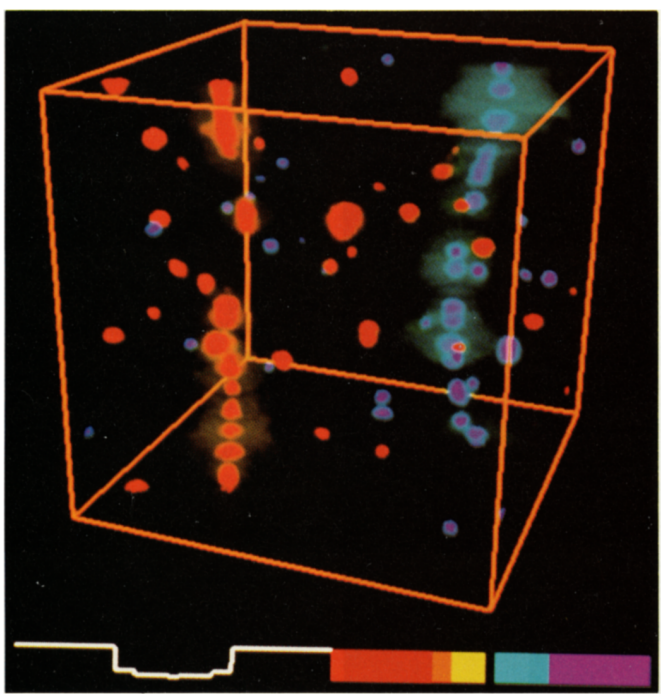

(b)

FIG. 8. q visualization approaching the end-states: (a) 2D plane with opaque rendering at $t=200$, and (b) QG in its volume with hazy rendering at $t=50$.

J. C. McWilliams and J. B. Weiss (see page 310)